Increased RhoA pathway activation downstream of αIIbβ3/SRC contributes to heterozygous Bernard Soulier syndrome

Larissa Lordier,[1-4*] Christian A. Di Buduo,[5*] Alexandre Kauskot,[6] Nathalie Balayn,[2-4] Cécile Lavenu-Bombled,[7] Francesco Baschieri,[8] Valérie Proulle,[9,10] Cecilia P. Marin Oyarzun,[2-4] Francesca Careddu,[5] Ida Biunno,[11] Tudor Manoliu,[4,12] Philippe Rameau,[4,12] Isabelle Plo,[2-4] Nicolas Papadopoulos,[13,14] Stefan Constantinescu,[13-16] William Vainchenker,[2-4] Guillaume Nam Nguyen,[17] Paola Ballerini,[17] Remi Favier,[17] Alessandra Balduini[5,18] and Hana Raslova[2-4]

[1]INOVARION, Paris, France; [2]INSERM UMR1287, Gustave Roussy, Equipe labellisée Ligue Nationale Contre le Cancer, Villejuif, France; [3]Université Paris-Saclay, UMR 1287, Gustave Roussy, Villejuif, France; [4]Gustave Roussy, UMR 1287, Villejuif, France; [5]Department of Molecular Medicine, University of Pavia, Pavia, Italy; [6]INSERM U1176, Hemostasis, Inflammation and Thrombosis (HITh), Université Paris-Saclay, Le Kremlin-Bicêtre, France; [7]Paris Saclay University, INSERM U1176 (HITh), AP-HP, Hematology Department, Bicêtre Hospital, Le Kremlin-Bicêtre, France; [8]Institute of Pathophysiology, Biocenter, Medical University of Innsbruck, Innsbruck, Austria; [9]Service Hématologie Biologique, Hôpital Cochin, AP-HP Centre - Université Paris Cité, France; [10]Unite INSERM UMRS 1138, CRC, Paris, France; [11]Integrated Systems Engineering, Bresso-Milano, Italy; [12]UMS AMMICa 23/3655, Plateforme Imagerie et Cytométrie, Gustave Roussy, Université Paris-Saclay, Villejuif, France; [13]Ludwig Institute for Cancer Research, Brussels, Belgium; [14]Université Catholique de Louvain and de Duve Institute, SIGN Unit, Brussels, Belgium; [15]Walloon Excellence in Life Sciences and Biotechnology, Brussels, Belgium; [16]Ludwig Institute for Cancer Research, Nuffield Department of Medicine, Oxford University, Oxford, UK; [17]Assistance Publique-Hôpitaux de Paris, Hôpital Armand Trousseau, Centre de Référence des Pathologies Plaquettaires, Paris, France and [18]Department of Biomedical Engineering, Tufts University, Medford, MA, USA

**LL and CADB contributed equally as first authors.*

Correspondence: H. Raslova
Hana.Raslova@gustaveroussy.fr

Received: August 9, 2024.
Accepted: February 28, 2025.
Early view: March 6, 2025.

https://doi.org/10.3324/haematol.2024.286424

Abstract

Bernard Soulier syndrome (BSS) is a severe bleeding disorder with moderate to severe thrombocytopenia, giant platelets, and platelet dysfunction, caused by biallelic mutations in *GP1BA, GP1BB,* or *GP9* genes. We generated induced pluripotent stem cells (iPSC) from a BSS patient with a novel heterozygous *GP1BA* p.N103D mutation, resulting in moderate macrothrombocytopenia. The mutation does not affect megakaryocyte (MK) differentiation or GPIb-GPIX complex expression but reduces affinity to von Willebrand factor (VWF). It induces increased signaling independent of VWF and αIIbβ3-mediated outside-in signaling, causing a profound defect in proplatelet formation after adhesion on fibrinogen. Pre-activation of αIIbβ3 integrin and heightened stress fiber formation linked to RhoA pathway overactivation were observed, likely due to increased phosphorylation of SRC at Y419 downstream of GPIbα. Dasatinib, a SRC inhibitor, restored stress fiber formation. Using a 3D bone marrow model to mimic platelet release under flow, we demonstrated that the ROCK1/2 inhibitor Y27632 increased platelet number and restored platelet size in GPIbα^{N103D} MK, as well as in MK from two other patients with heterozygous *GP1BA* mutations (p.L160P and p.N150S). However, Y27632 had no additional effect on platelet generation from MK of two patients with biallelic BSS, suggesting a distinct molecular mechanism in biallelic cases.

Introduction

Bernard Soulier syndrome (BSS; MIM #231200) is an autosomal recessive disorder due to quantitative or qualitative defects of the GPIb-IX complex with a severe bleeding diathesis. Presently, more than 50 missense, nonsense or frameshift mutations have been reported in *GP1BA, GP1BB* or *GP9* genes coding for GPIbα, GPIbβ and GPIX, while no

defect has been found in the *GP5* gene, coding for the GPV subunit.[1] BSS is characterized by moderate to severe thrombocytopenia, giant platelets, and platelet dysfunction, and has an estimated incidence of 1/1,000,000. Although it was reported that giant platelets could be related to defects in proplatelet formation (PPF) from patient megakaryocytes (MK), the precise mechanisms leading to macrothrombocytopenia are unknown.

A few cases with autosomal dominant transmission (monoallelic BSS) and mild bleeding have also been described. *GP1BA*^{A156V} (or p.A172V) also called Bolzano mutation is the most frequent heterozygous mutation.[2,3]

The role of glycoprotein GPIb-IX complex in platelet functions is well established. Its interaction with von Willebrand factor (VWF) plays a major role in platelet adhesion and plug formation at sites of vascular injury. However, its involvement in regulating platelet production remains poorly understood. The use of *Gp1ba* and *Gp1bb* knockout (KO) mice revealed a role of this receptor during the final stages of MK maturation, notably the formation of the demarcation membrane system (DMS) and proplatelet extension,[4,5] likely independently of VWF since *Vwf* KO mice display no MK poiesis defect.[6] Similarly, human MK derived from induced pluripotent stem cells (iPSC) of homozygous BSS patients carrying mutations in *GP1BA* or *GP1BB*, did not express the GPIb-GPIX complex on their cell surface. This led to the production of abnormally large proplatelets and macroplatelet-like particles with a dilated DMS,[7] mirroring the findings in mice.

In platelets, it is well established that VWF binding to the GPIb-IX complex initiates platelet activation turning on several signaling pathways such as Src family kinases (Lyn and Src), SYK, Rac1, PI3-kinase/Akt, BAD, cGMP-dependent protein kinase and MAP kinases.[8-10] Indeed, the interaction of the intracytoplasmic domain of GPIbα with 14-3-3ζ, after VWF binding, initiates a signaling cascade leading to integrin αIIbβ3 activation.[11] However, less is known about GPIb-GPIX-mediated signaling in the MK lineage. It has been shown that the absence of the cytoplasmic tail of GPIbα prevents 14-3-3ζ interaction and phosphorylation of AKT, which could impair thrombopoietin-mediated responses.[12] However, this does not explain the defect in DMS and the presence of macrothrombocytopenia in BSS. The interaction between GPIbα with cytoskeleton proteins and mainly with filamin A (FLNa) was proposed as regulator of platelet formation and size in mouse models[5,13-15] but only a slight effect on *in vitro* PPF was detected in the absence of GPIbα/FLNa interaction in human MK derived from iPSC induced from patients with filaminopathy A,[16] suggesting that other mechanisms could be involved.

In heterozygous BSS, the Bolzano Ala156Val mutation was shown to reduce PPF by half.[17] However, the mechanism by which mutations in the extracellular domain of GPIbα, while maintaining intracellular interactions, lead to such a defect, has not been explored. Here, we derived iPSC from a BSS patient with a novel heterozygous mutation in the extracellular leucine-rich repeats (LLR) domain of *GP1BA* *GP1BA*^{N103D}, resulting in mild macrothrombocytopenia. We report an overactivation in the RhoA pathway due to increased SRC phosphorylation. Employing a 3D bone marrow model to simulate platelet release under flow conditions,[18,19] we demonstrate that ROCK1/2 inhibition restores platelet number and size for heterozygous BSS patients with mutations in the extracellular LRR domain of *GP1BA* but not for homozygous BSS patients with a homozygous mutation in the extracellular LRR domain of *GP1BA* or *GP1BB*.

Methods

Study approval

Blood samples from patients and healthy subjects were collected after informed written consent and obtained in accordance with the Declaration of Helsinki. The study was approved by the Comité de Protection des Personnes CPP N°2020T2-02, France.

Five unrelated individuals (P1-P5) were identified with macrothrombocytopenia during routine blood tests (*Online Supplementary Table S1*).

Induced pluripotent stem cell generation and expansion

CD34$^+$ cells obtained from peripheral blood of P1 patient were cultured in a serum-free medium supplemented with cytokines for 6 days and transduced using the CytoTune iPS 2.0 Sendai Reprogramming Kit (Thermo Fisher).

Flow cytometry

Single cell suspensions were subjected to staining using monoclonal antibodies directly coupled to their respective fluorochromes. Analysis was conducted using BD Canto II or BD LSRFortessa cytometers (BD Biosciences). MK were isolated on Influx, ARIA III, or ARIA Fusion cell sorters (BD Biosciences).

Silk bone marrow model

Silk fibroin aqueous solution was obtained from *B. mori* silkworm cocoons according to previously published literature.[20] Silk scaffolds have been produced by a salt-leaching method, as previously described.[21] The dynamic perfusion of the 3D silk bone marrow model was performed by using a peristaltic pump (ShenChen Flow Rates Peristaltic Pump - LabV1) connected to a bioreactor chamber manufactured using 3D SLA printing technology (Form 3B, Formlab) and consisted of two wells each of which was equipped with a 3D silk fibroin scaffold; 1.5×10^5 MK were seeded into each silk scaffold and kept at 37 °C and 5% CO2.

Statistics

All data are shown as mean ± standard error of mean (SEM), mean ± standard deviation (SD) or mean ± minimum to maximum. The statistical analyses were performed using

the PRISM software. Statistical significance was established using a Student's *t* test or a one-way analysis of variance (ANOVA) specified in legends. Differences were considered significant at $P<0.05$.

Results

To investigate the mechanism of macrothrombocytopenia in patients with monoallelic *GP1BA* mutation, we derived iPSC from a female patient with mild macrothrombocytopenia (P1, 118x10^9 platelets/L) and rare hemorrhagic manifestations such as epistaxis and ecchymosis. The patient exhibited a slight defect in platelet aggregation (70-80% response to ADP, EPI, COL, AA, TRAP and ristocetin) and carried a new heterozygous p.N103D mutation in the extracellular LLR4 domain of the *GP1BA* gene that was initially identified by next-generation sequencing (NGS) and confirmed by Sanger sequencing (*Online Supplementary Figure S1; Online Supplementary Table S1*). For these reasons, the patient was classified as monoallelic Bernard Soulier syndrome. Three different clones were characterized and utilized for subsequent studies (*Online Supplementary Figure S2*). Additionally, three previously described independent iPSC lines were employed as controls.[22-24]

GPIbα^{N103D} expression in megakaryocytes

MK were differentiated from iPSC using a previously described protocol.[16] The cell surface expression levels of αIIb (CD41), GPIX (CD42a), and GPIbα (CD42b) in MK were unaffected by the presence of the *GP1BA*^{N103D} mutation (Figure 1A), as well as their total cellular level as shown by western blot analysis (Figure 1B; *Online Supplementary Figure S3A*). In computational modeling, the 3D structure of the GPIbα^{N103D} mutant remained unaffected (Figure 1C). Immunological staining of MK showed no difference in GPIbα distribution (Figure 1D; *Online Supplementary Figure S3B*).

Normal maturation of GPIbα^{N103D} megakaryocytes

GPIbα^{N103D} did not affect the ploidy level (*Online Supplementary Figure S3C*). Electronic microscopy revealed no defect in maturation with normal DMS and α-granule formation (*Online Supplementary Figure S3D*), as also attested by the immunostaining of GPIbα, actin (Figure 1D) and VWF (*Online Supplementary Figure S3E*). A slight increase in actin distribution on the cell membrane was detected (*Online Supplementary Figure S3B*). GPIbα has been proposed to regulate DMS and PPF formation through its interaction with the cytoskeleton, particularly FLNa. However, filamin distribution was similar to that observed in control MK (Figure 1D; *Online Supplementary Figure S3B*), and the co-immunoprecipitation assay performed with anti-GPIBα antibody revealed no defect in the interaction between GPIbα and FLNa (Figure 1E). A trend towards reduced MK activation in response to thrombin was observed, with a significant decrease at 0.5 U/mL, as indicated by the membrane expression of P-selectin (Figure 1F).

Abnormal proplatelet formation by GPIbα^{N103D} megakaryocytes

We then investigated proplatelet formation by mutant *versus* control MK in a liquid culture containing thrombopoietin (TPO) and stem cell factor (SCF). No difference in the percentage of proplatelet-forming MK was detected (Figure 2A). The analysis of proplatelets revealed an increased size of tips with a slight decrease in the distribution of GPIbα on the tips and decreased GPIbα level at the surface of platelet-like particles generated *in vitro* (*Online Supplementary Figure S4A-C*). This is consistent with a slight increase in GPIbα shedding during proplatelet formation (*Online Supplementary Figure S4D*). After adhesion on fibrinogen (20 mg/mL) for 72 hours, a 2.5-fold decrease in the percentage of MK forming proplatelets was detected (Figure 2B).

To accurately assess the differences in both quantity and size of platelets produced by mutant and control samples, CD41$^+$CD42$^+$ mature MK were introduced into a 3D bone marrow model made of silk fibroin and functionalized with 50 μg/mL fibrinogen. The system was perfused for 6 hours with culture medium to collect platelets, which were then quantified using flow cytometry (Figure 2C). Platelet diameters were measured after adhesion on polylysine-coated slides using Arivis Vision 4D (Zeiss). Compared to controls, 3.35-times fewer platelets were recovered from GPIbα^{N103D} MK (Figure 2D), and their size was significantly larger (Figure 2E), confirming that MK derived from patient-specific iPSC replicate the characteristics of BSS. The increased size of platelets was also confirmed by electron microscopy (Figure 2F). A 1.57-fold reduction in platelet numbers was also observed when the 3D bone marrow model was functionalized with 50 μg/mL fibronectin (*Online Supplementary Figure S4D, E*). Interestingly, only a slight increase in platelet size was detected (*Online Supplementary Figure S4D, F*) suggesting that the macrothrombocytopenia depends primarily on fibrinogen activation on αIIbβ3.

Decreased von Willebrand factor binding in the presence of GPIbα^{N103D} mutant

To understand how the GPIbα^{N103D} mutant affects receptor function and platelet aggregation, we first investigated the adhesion of MK on VWF. The adhesion of CD41$^+$CD42$^+$ MK on VWF for 30 min was not affected (*Online Supplementary Figure S5A*). However, when cells were incubated with ristocetin (0.5 mg/mL) and different concentrations of soluble VWF for 30 min, decreased sensitivity was detected by flow cytometry in the presence of a low dose (0.1 mg/mL of VWF) (*Online Supplementary Figure S5B*). The specificity of the binding of VWF (0.1 mg/mL) to the GPIb complex was confirmed after incubation with a blocking anti-CD42b

antibody (*Online Supplementary Figure S5C*). These results show that like other BSS monoallelic mutations that are not predicted to bind VWF,[25] GPIbα p.N103D decreases the affinity of the GPIbα-GPIX receptor for VWF.

Increased RhoA activation in GPIbα^{N103D} megakaryocytes

Next, we assessed whether the GPIbα^{N103D} mutant could affect αIIbβ3-mediated signaling in MK. We examined the activation of αIIbβ3 under basal conditions and after ac-

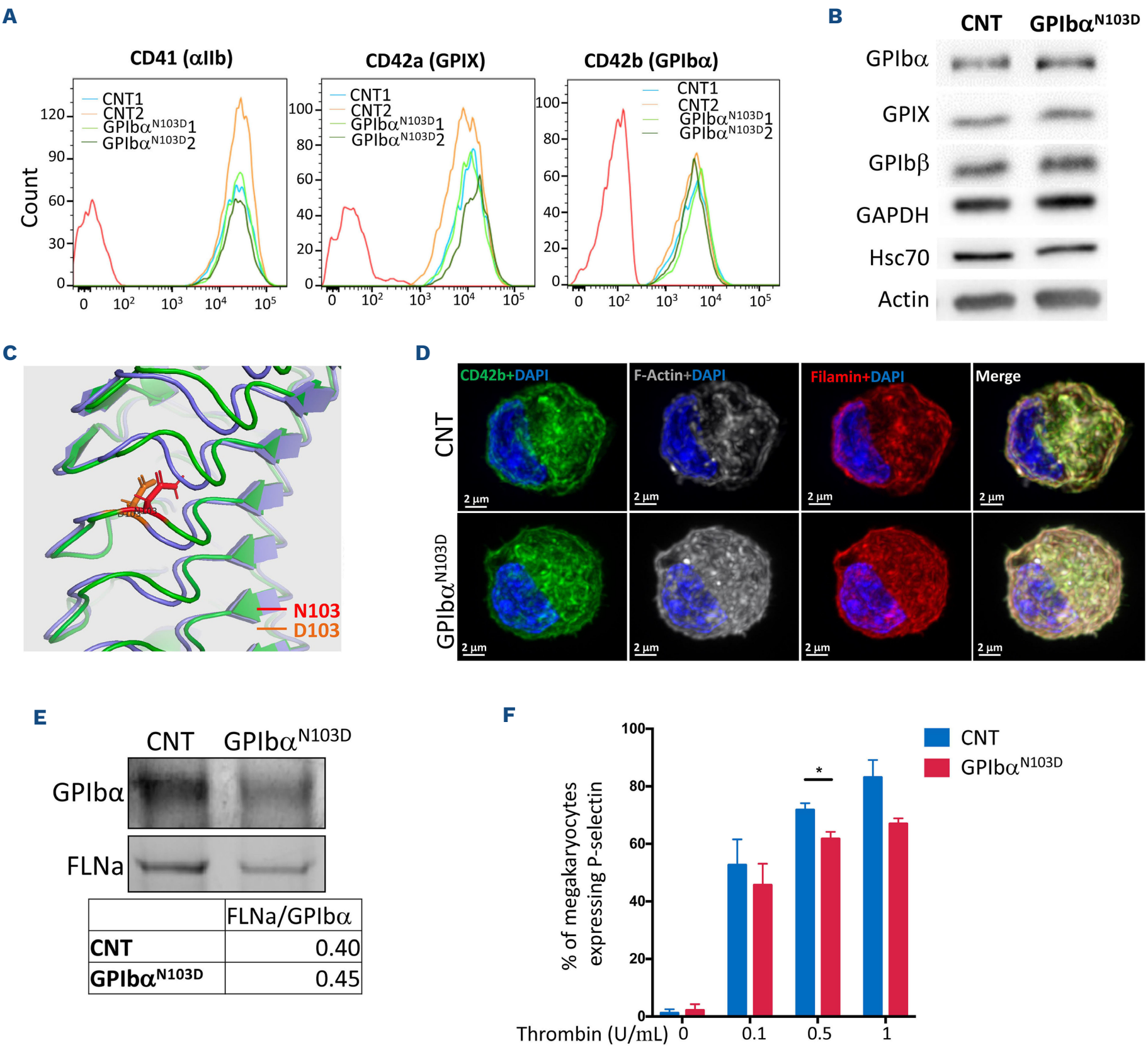

Figure 1. GPIbα^{N103D} mutant does not affect megakaryocyte differentiation from iPSC. (A) Flow cytometry plots showing expression of CD41, CD42a and CD42b on control (CNT1, CNT2) and GPIbα^{N103D} (2 different clones were used) megakaryocytes (MK). (B) Representative western blot of GPIb-GPIX complex (GPIbα, GPIbβ, GPIX) on mature control (CNT) and GPIbα^{N103D} MK. GAPDH, HSC70 and actin were used as loading controls. Quantification is shown in *Online Supplementary Figure S3A*. (C) 3D structure predicted by using AlphaFold Protein Structure Database (https://alphafold.ebi.ac.uk/entry/P07359). hGPIbα wild-type and hGPIbα^{N103D} mutants aligned, focus on N/D103. (D) Representative immunofluorescence staining pictures of mature control (CNT) an GPIbα^{N103D} MK: GPIbα (CD42b, green), F-actin (gray), filamin A (red), DAPI (nuclei, blue). Scale bar: 2 mm, z-stack middle frame is shown. (E) Co-immunoprecipitation assay performed on control (CNT) and GPIbα^{N103D} MK confirming the interaction between GPIbα and filamin A (FNLa). Mouse anti-GPIbα was used for immunoprecipitation and both anti-GPIbα and rabbit anti-FLNa antibodies were used for western blot assay. The quantification revealed no defect in the GPIbα-FLNa interaction in presence of GPIbα^{N103D} mutant. (F) Flow cytometry analysis of P-selectin at cell surface after activation of MK with indicated concentration of thrombin for 5 minutes. Anti-P-selectin antibody conjugated with PE was used. Data represent the mean ± standard error of the mean, N=3; *P<0.05, paired t test.

tivation with thrombin. In the basal state, integrins predominantly exist in an inactive state on the cell surface until they receive an external signal. In basal condition, incubation of MK with the PAC1 antibody, directed against the active αIIbβ3 conformation, or with fibrinogen-FITC showed no significant difference in PAC1 and fibrinogen binding between GPIbα^{N103D} mutant and control MK, respectively (*Online Supplementary Figure S6A, B*; Figure 3A). To investigate whether the GPIbα^{N103D} mutant could induce increased pre-activation of the αIIbβ3 complex, MK were activated with thrombin (1 U/mL) for 5 min and then incubated either with PAC-1 or with fibrinogen-FITC. As

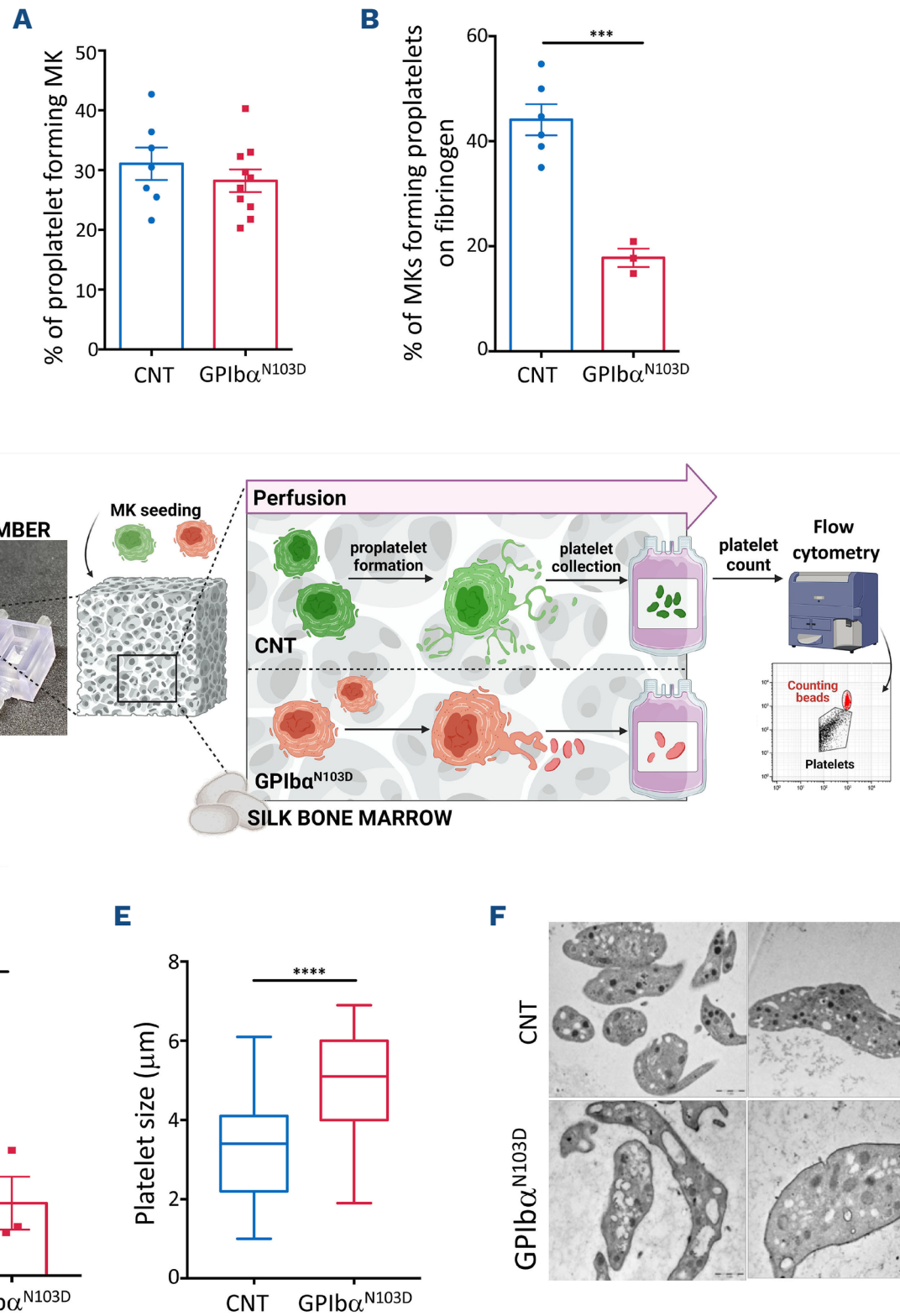

Figure 2. GPIbα^{N103D} mutant alters proplatelet formation and platelet generation. (A) Frequency of proplatelet forming control (CNT) and GPIbα^{N103D} mutant megakaryocytes (MK) cultured in liquid medium in presence of thrombopoietin (TPO) and stem cell factor (SCF). Data are expressed as mean ± standard error of the mean (SEM) (CNT N=7, GPIbα^{N103D} N=10). (B) Frequency of proplatelet forming control (CNT) and GPIbα^{N103D} mutant MK on after adhesion of slides coated with 20 mg/mL of fibrinogen. Data are expressed as mean ± SEM (CNT N=6, GPIbα^{N103D} N=3); ***P<0.001, unpaired t test. (C) Schematic representation of *ex vivo* platelet collection from MK cultured into the silk bone marrow model functionalized with fibrinogen (50 μg/mL); 1.5x10^5 control (CNT) and GPIbα^{N103D} mutant MK were seeded into scaffolds. Samples were perfused with culture medium, into a multi-well flow chamber, for 6 hours. Released platelets were collected into gas-permeable bags. Samples were mixed with counting beads to quantify the number of platelets that were identified as CD41$^+$CD42a$^+$ events. (D) The number of recovered platelets is shown. Data are expressed as mean ± SEM (CNT N=3, GPIbα^{N103D} N=3); *P<0.05, unpaired t test. (E) Platelet diameters (mm) of *ex vivo*-released platelets were measured by Arivis Vision 4D (Zeiss). Data are expressed as mean ± minimum to maximum, CNT N=127, GPIbα^{N103D} N=136; ****P<0.0001, unpaired t test. (F) Transmission electron microscopy of *ex vivo* produced platelets (scale bar: 2 μm).

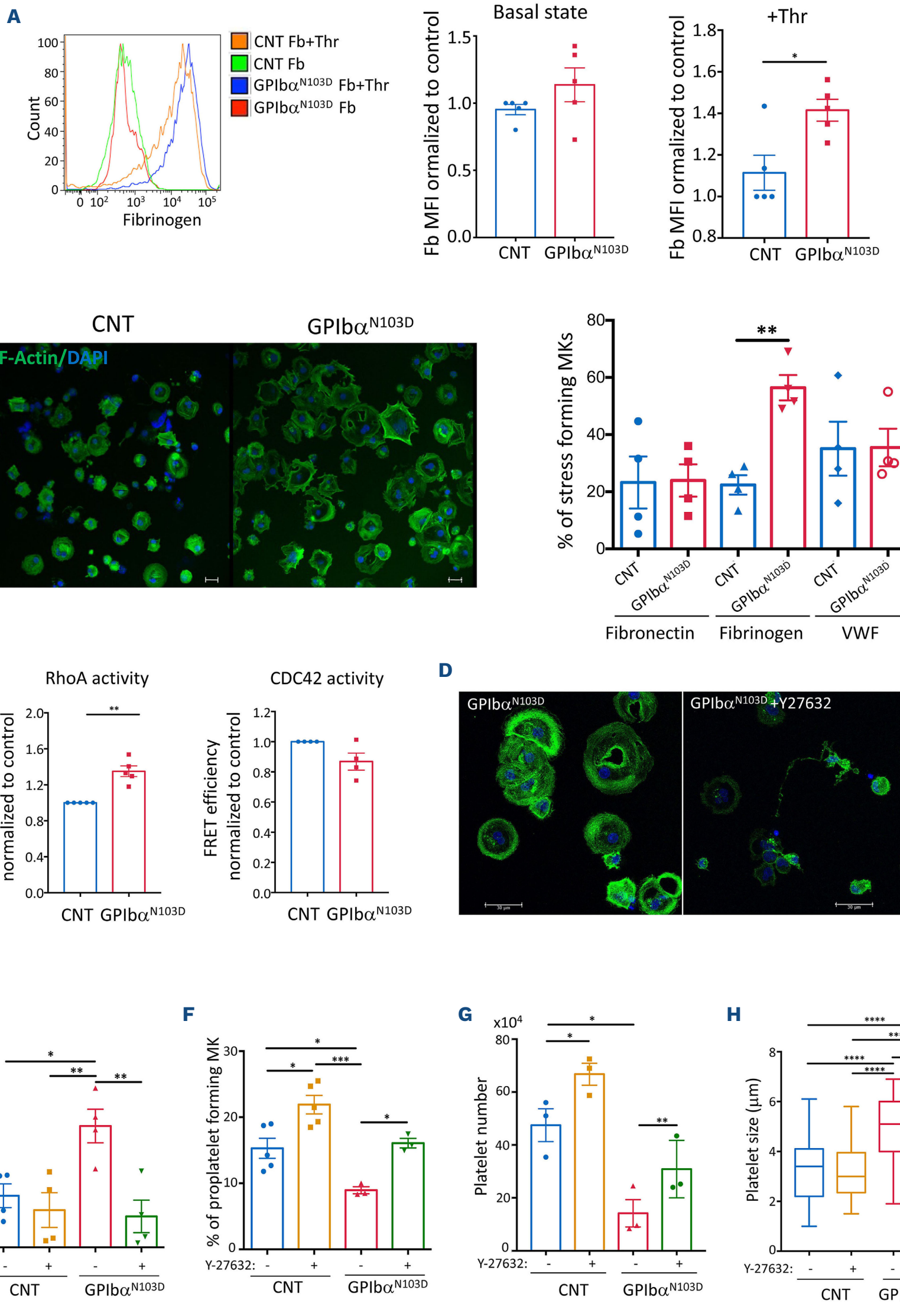

Figure 3. GPIbα^{N103D} mutant induces an increase in RhoA activity downstream aIIbβ3. (A) Flow cytometry analysis fibrinogen (Fb) binding to aIIbβ3 receptor on control (CNT) and GPIbα^{N103D} mutant megakaryocytes (MK) before and after its activation by thrombin (Thr). MK were stimulated or not for 5 minutes with thrombin (1 U/mL) and then incubated with Alexa 488-conjugated fibrinogen. Representative picture of plots is shown on the left panel. The histogram presenting the mean fluorescence intensity (MFI)

Continued on following page.

of fibrinogen (Fb) staining at basal state is shown on the middle panel and after stimulation by thrombin on the right panel. The MFI after stimulation was normalized to the corresponding condition without stimulation. The histograms present the MFI of Fb normalized to 1 control in each experiment. Three independent experiments are shown. Data are expressed as mean ± standard error of the mean (SEM) (CNT N=5, GPIbα^{N103D} N=5); *P<0.05, Mann-Whitney test. (B) Spreading assay of mature control (CNT) and GPIbα^{N103D} mutant MK plated on different substrates. Representative picture of immunofluorescence staining of MK plated on fibrinogen-coated surface and stained for F-actin (green) and DAPI (blue) is shown on the left panel, single z-stack frame at the glass adhesion site is shown. The histogram presenting the frequency (%) of stress fiber forming MK plated on fibrinogen-, von Willebrand factor (VWF)- or fibronectin-coated surface is shown on the right panel. Data are expressed as mean ± SEM, N=4; **P<0.01, paired *t* test. (C) FRET analysis for RhoA or Cdc42 activation on fibrinogen-coated surface. At least 15 cells per condition were analyzed in each experiment. The histograms represent the average of 4-5 independent experiments. Data are normalized to control condition (CNT) for each experiment and are expressed in arbitrary units (a.u.) as mean ± SEM, N=5 for RhoA, N=4 for CDC42; **P<0.01, Mann-Whitney test. (D, E) Immunofluorescence analysis of stress fibers formation by mature control (CNT) and GPIbα^{N103D} mutant MK. Mature MK were plated on fibrinogen-coated surface in presence or absence of ROCK1/2 inhibitor Y27632 for 30 minutes and stained for F-actin (green) and DAPI (blue). (D) Representative pictures of immunofluorescence staining. Scale bar: 30 μm, single z-stack frame at the glass adhesion site is shown. (E) The histogram presenting the frequency (%) of stress fiber forming MK plated on fibrinogen-coated surface. Data are expressed as mean ± SEM, N=4; *P<0.05; **P<0.01, one-way analysis of variance (ANOVA) with Tukey's multiple comparison method was used. (F) Immunofluorescence analysis of proplatelet formation by mature control (CNT) and GPIbα^{N103D} mutant MK. The histogram presenting the frequency (%) of proplatelet forming MK plated on the fibrinogen-coated surface in the presence or absence of ROCK1/2 inhibitor Y27632, for 24 hours. Data are expressed as mean ± SEM, CNT N=5, GPIbα^{N103D} N=3; *P<0.05; ***P<0.001, one-way ANOVA with Tukey's multiple comparison method was used. Representative pictures of immunofluorescence staining are shown in SF 7B. (G, H) 1.5x10^5 MK were seeded in the silk scaffolds for 48 hours with or without the ROCK1/2 inhibitor Y27632, perfused with culture media for 6 hours, and released platelets were collected into gas-permeable bags. (G) The histogram represents the number of *ex vivo*-released platelets. Samples were mixed with counting beads to quantify the number of platelets identified as CD41$^+$CD42a$^+$ events. Data are expressed as mean ± SEM, N=3; *P<0.05; **P<0.01, paired *t* test. (H) Platelet diameters (mm) of *ex vivo*-released platelets with or without ROCK1/2 inhibitor Y27632 were measured by Arivis Vision 4D (Zeiss). Data are expressed as mean ± min to max, CNT N=127, CNT+Y27632 N=133, GPIbα^{N103D} N=136, GPIbα^{N103D} +Y27632 N=127; ****P<0.0001, one-way ANOVA with Tukey's multiple comparison method was used. Representative pictures of *ex vivo*-released platelets with or without ROCK1/2 inhibitor Y27632 are shown in *Online Supplementary Figure S7C*.

depicted in Figure 3A, a slight but significant increase in fibrinogen binding was detected for the mutated MK after activation with thrombin and a similar tendency was detected for PAC-1 (*Online Supplementary Figure S6A, C*). To confirm that the GPIbα^{N103D} mutant induces unusual αIIbβ3 activation, MK were plated onto a fibrinogen matrix for 30 min, and cell morphology was analyzed by fluorescence microscopy after labeling the F-actin network. GPIbα^{N103D} led to an increased spreading with a higher percentage of MK forming stress fibers (56.4% for mutant MK *vs*. 22.4% for control MK) (Figure 3B). This increased stress fiber formation was not observed after adhesion onto fibronectin and VWF. This suggests that although no increased αIIbβ3 activation was detected by flow cytometry under basal conditions, the GPIbα^{N103D} mutant may prime αIIbβ3 for activation in the absence of VWF. Interestingly, thrombin stimulation significantly increased the percentage of stress fiber-forming MK in the control group, rising from 20.3% to 50.6%, which matched the frequency of spread MK observed in GPIbα^{N103D} mutant MK without stimulation (*Online Supplementary Figure S6D*). The effect was even more pronounced in GPIbα^{N103D} mutant MK, where the percentage increased from 41.6% to 81.6%.

Stress fiber formation being a hallmark of RhoA activation, we further focused on RhoA pathway. Using a lentiviral FRET biosensor based on the Raichu probe,[16] we measured RhoA activity. A slight but significant increase in RhoA activity was detected in GPIbα^{N103D} MK after adhesion to fibrinogen compared to controls (Figure 3C). This finding matches with the mild macrothrombocytopenia induced by this mutant. Previously, it was demonstrated that the GPIb-GPIX complex regulates the balance between RhoA and CDC42 signaling.[26] Therefore, we also measured CDC42 activity under the same conditions and observed a slight decrease in CDC42 activity (Figure 3C), confirming that the GPIbα^{N103D} mutant deregulates the RhoA/CDC42 balance.

Inhibition of RhoA pathway restores stress fiber formation, platelet production and platelet size

The main RhoA effector that regulates acto-myosin cytoskeleton reorganization through myosin light chain 2 (MLC2) phosphorylation in MK is the Rho-associated kinase (ROCK). To assess its overactivation in GPIbα^{N103D} MK, we first investigated the localization of P-MLC2 and demonstrated its co-localization with F-actin during abnormal stress fiber formation after adhesion to fibrinogen (*Online Supplementary Figure S7A*). Notably, treatment of MK with the Y27632 ROCK1/2 inhibitor resulted in a 3.9-fold decrease in the proportion of stress fiber-forming MK (Figure 3D, E) after adhesion to fibrinogen for 30 min.

ROCK1/2 inhibition increased the percentage of proplatelet-forming GPIbα^{N103D} MK after adhesion to fibrinogen to a level close to normal MK (Figure 3F; *Online Supplementary Figure S7B*). To precisely quantify the impact of ROCK1/2 inhibition on platelet production and platelet size, MK were seeded in the 3D silk bone marrow model functionalized with fibrinogen and incubated or not with Y27632. This niche mimic was housed in a perfusable chamber. The flow through

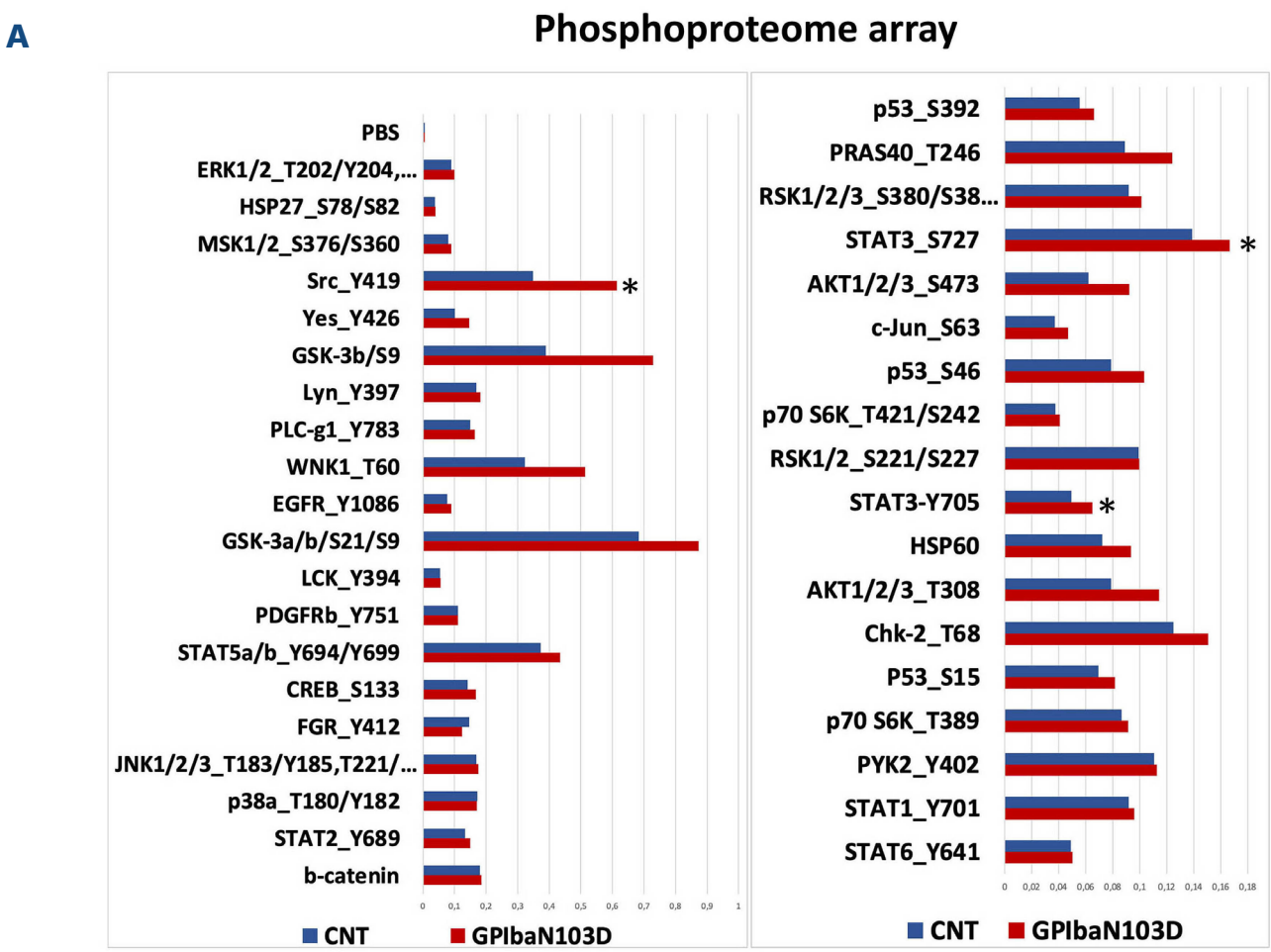

Figure 4. Mechanism of RhoA pathway activation. (A) Phosphoproteome analysis of control (CNT) and GPIbα^{N103D} mutant megakaryocytes (MK). Mature MK were seeded on fibrinogen-coated surface for 30 minutes (min), lysed and were analyzed using membrane-based human phospho-kinase antibody array. One of 2 experiments is shown. (B) Western blot analysis of P-SRC Y419 and P-STAT3 Y705 in control (CNT) and GPIbα^{N103D} mutant MK after 30 min incubation on fibrinogen-coated surface. Immunoblots

Continued on following page.

were probed with monoclonal antibodies directed against P-STAT3 Y705, P-SRC Y419, STAT3, SRC and actin as loading control. Representative picture of immunoblot is shown on the left. Quantification of P-STAT3 Y705/total STAT3 is shown in the middle panel and that of P-SRC Y419/total SRC on the right panel. The ratios for mutant GPIbα^{N103D} MK were normalized to control MK. Data are expressed as mean ± minimum to maximum, P-STAT3 N=7, P-SRC N=8; *P<0.05, unpaired t test. (C-E) Effect of dasatinib on MK spreading. Control (CNT) and GPIbα^{N103D} mutant MK were incubated in presence of dasatinib (10 μM) for 15 min and plated on fibrinogen-coated surface for 30 min. (C) Western blot on MK showing a decrease in P-SRC Y419 in CNT and GPIbα^{N103D} mutant MK incubated with dasatinib. (D) Representative pictures of stress fiber forming MK stained with F-actin (green) and DAPI (blue). Scale bar: 30 μm, single z-stack frame at the glass adhesion site is shown. (E) Frequency of stress fiber forming MK. Data are expressed as mean ± standard error of the mean, CNT N=3, GPIbα^{N103D} N=4; *P<0.05; **P<0.01, one-way analysis of variance (ANOVA) with Tukey's multiple comparison method was used.

the scaffold enabled platelets to detach and release into the perfused culture medium, with or without Y27632. Platelets were collected into a collection bag, and their number was estimated using flow cytometry with counting beads. Incubation with Y72632 led to a 2.2-fold increase in the platelet count generated by GPIbα^{N103D} MK, a level close to normal MK with a partial correction of platelet size (Figure 3G, H; *Online Supplementary Figure S7C*). A 1.4-fold increase in the platelet number was also detected for normal MK.

GPIbα^{N103D} mutant induces increased P-SRC Y419 and P-STAT3 Y705 levels

How GPIb precisely regulates the RhoA pathway in MK remains unclear. The GPIba is linked through its cytoplasmic domain to proteins necessary for the DMS formation, such as PACSIN2 and FLNa.[15] Additionally, its interaction with the adaptor protein 14-3-3z activates a signaling cascade leading to αIIbβ3 activation in platelets. The GPIbα^{N103D} mutation does not affect FLNa interaction and DMS formation. To gain further insights into the mechanism by which this mutant could activate the RhoA pathway, we performed a phosphoproteome analysis on MK after adhesion to fibrinogen. Two independent experiments revealed increased phosphorylation of different proteins, including SRC at tyrosine Y419 and STAT3 on tyrosine Y705 and serine S727 (Figure 4A; *Online Supplementary Figure S8*). SRC has been reported to activate GEF-H1 either directly or indirectly through STAT3 phosphorylation at tyrosine Y705, both leading to the release GEF-H1 from microtubules and allowing RhoA activation.[27-29] Hence, we confirmed increased phosphorylation of STAT3 at Y705 and SRC at Y419 by western blot (Figure 4B). Finally, when phosphorylation of SRC was inhibited using a non-specific SRC inhibitor dasatinib (Figure 4C), a 2.14-fold decrease in the frequency of stress fiber-forming MK was detected (Figure 4D, E).

RhoA inhibition restores platelet production from heterozygous but not homozygous Bernard Soulier syndrome

To confirm the implication of the RhoA pathway in heterozygous BSS, we examined the effect of the ROCK1/2 inhibitor Y27632 on *in vitro*-derived megakaryopoiesis and platelet generation in two patients carrying *GP1BA*^{L160P} (P2) and *GP1BA*^{N150S} (P3) mutations in LRR6, respectively. MK differentiation (Figure 5A; Figure 6A) and the expression of αIIb (CD41) and the GPIb-GPIX complex (CD42) at the cell surface (Figure 5B; Figure 6B) were not affected. On day 10 of culture CD41^{+}CD42^{+} MK were sorted, seeded into the 3D bioreactor (Figure 5C; *Online Supplementary Figure S9*), and perfused into the flow chamber to collect platelets. A 2.12-fold increase in platelet yield was detected for P2, compared to a 1.48-fold increase for control platelets after incubation with the ROCK1/2 inhibitor (Figure 5D).

The inhibition of the RhoA pathway led to a 1.3-fold decrease in platelet size for P2 and a 1.19-fold decrease for control platelets (CNT2) (Figure 5E). For P3, the ploidy was also examined without detecting any defect (Figure 6C), and a 4.67-fold increase in platelet number was observed compared to a 1.48-fold increase for control platelets (CNT) (Figure 6D). The inhibition of the RhoA pathway led to a 1.32-fold decrease in platelet size for P3 while no decrease was detected for control platelets (CNT3) (Figure 6E). Overall, these results demonstrate that the inhibition of the RhoA pathway in heterozygous BSS partially restores the generation of normal-sized platelets. The effect of RhoA inhibition is more significant in the patients' samples than in controls, where RhoA is still activated but to a lesser degree, and thus its inhibition has a less pronounced effect on platelet generation.

Finally, we examined the effect of RhoA inhibition on homozygous BSS patients carrying homozygous *GP1BB*^{G43W} (P4) and *GP1BA*^{L139P} (P5) mutations, respectively. No defect in the frequency of MK was detected (*Online Supplementary Figure S10A, E*). However, while αIIb (CD41) expression at the cell surface of MK was normal, a substantial decrease in GPIb-GPIX complex (CD42) expression was observed for both patients (*Online Supplementary Figure S10B,F*). The modal ploidy level, measured only for P4, was also considerably decreased (N=6.9 for control MK *vs.* N=3.35 for patient MK) (*Online Supplementary Figure S10C*). A decreased frequency of proplatelet-forming MK was detected for P4, with no specific effect of RhoA inhibition, as shown by a 1.4-fold increase for control MK and a 1.38-fold increase for patient MK (*Online Supplementary Figure S10D*). For P5, the effect of RhoA inhibition on platelet production was evaluated in the 3D culture system, as for P2 and P3 (*Online Supplementary Figure S10G-I*). The number of platelets

generated by an identical number of MK was decreased, but no specific effect of RhoA inhibition was evidenced (*Online Supplementary Figure S10H*). The inhibition of the RhoA pathway led to only a 1.15-fold decrease in platelet size for P5 while no decrease was detected for control platelets (CNT) (*Online Supplementary Figure S10I*). These results indicate that RhoA inhibition does not restore platelet generation, suggesting, together with decreased ploidy for P4, that the mechanism of thrombocytopenia in homozygous BSS is not the same as in heterozygous BSS.

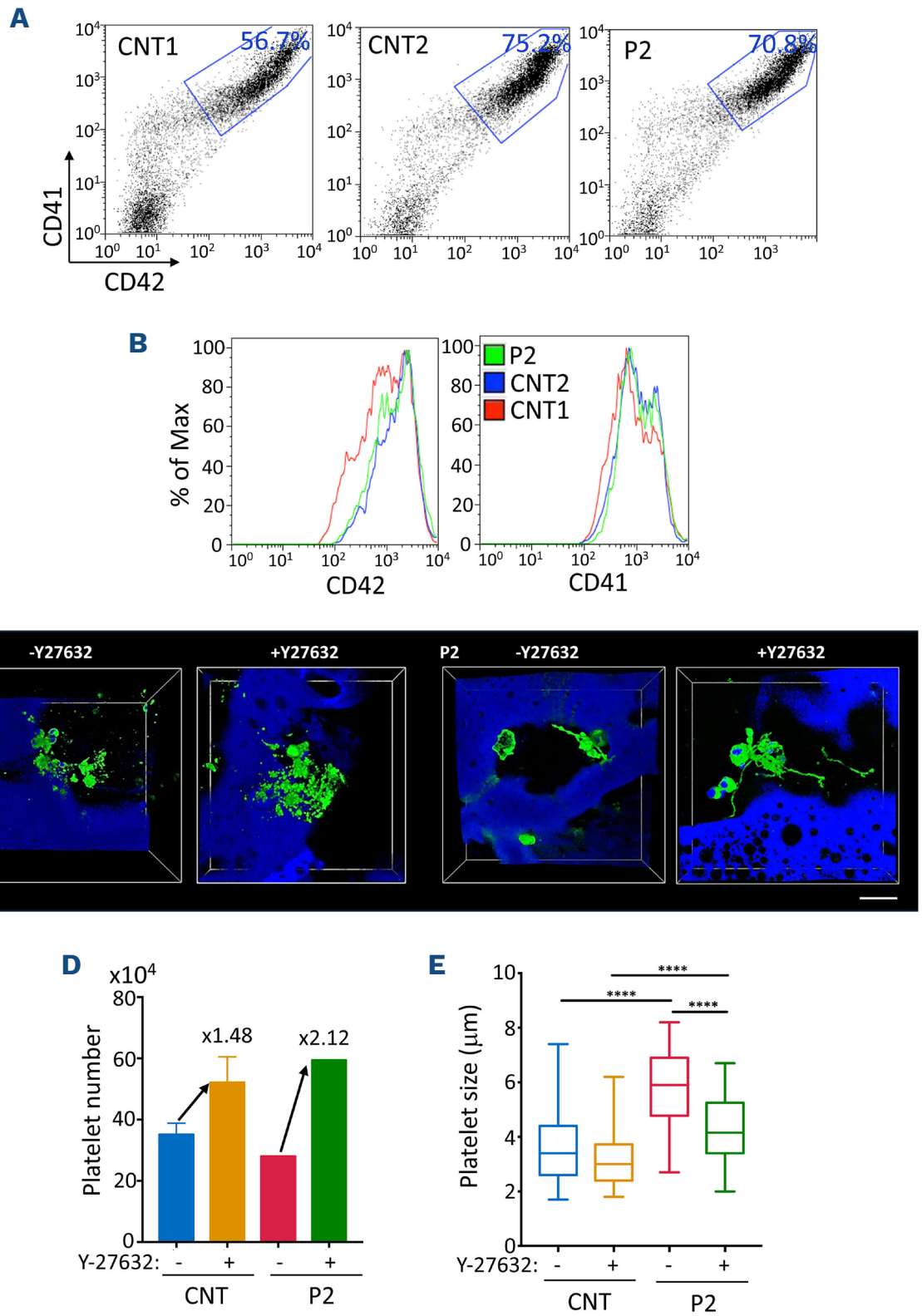

Figure 5. RhoA inhibition restores the platelet generation in heterozygous Bernard Soulier syndrome. Hematopoietic progenitors were isolated from peripheral blood of 3 healthy controls and 1 patient carrying heterozygous *GP1BA* p.L160P (P2) mutation, and cultured in presence of thrombopoietin (TPO) and stem cell factor (SCF) for 10 days. (A, B) Flow cytometry analysis of control (CNT1, CNT2) and patient 2 (P2) megakaryocytes (MK). (A) Percent of mature $CD41^+CD42^+$ MK. (B) CD41 and CD42 expression level. (C-E) MK were seeded into the silk sponge with or without ROCK1/2 inhibitor Y27632. (C) Representative picture of control (CNT2) and P2 proplatelet forming MK. MK and platelets are stained with anti-CD61 the antibody (green) and the silk sponge is in blue. Scale bar: 50 µm, full 3D volume is shown. (D) Silk scaffolds were perfused with culture media for 6 hours, and released platelets were collected into gas-permeable bags. Samples were mixed with counting beads to quantify the number of platelets, identified as $CD41^+CD42a^+$ events. The number of recovered platelets is shown. A 1.48-fold increase in platelet number was detected for controls after incubation with ROCK1/2 inhibitor (N=3, data are presented as mean ± standard deviation) and 2.12-fold increase for P2 after incubation with ROCK1/2 inhibitor. (E) Platelet diameters (mm) of *ex vivo*-released platelets with or without ROCK1/2 inhibitor Y27632 were measured by Arivis Vision 4D (Zeiss). Data are expressed as mean ± minimum to maximum, N=50; ****P<0.0001, one-way analysis of variance (ANOVA) with Tukey's multiple comparison method was used.

Discussion

In this study we have developed an iPSC-based model of monoallelic BSS that demonstrates i) the mechanism by which heterozygous *GP1BA* mutations lead to a defect in platelet production by activating the RhoA pathway, ii) that by using a 3D bone marrow model we can detect the rescue of platelet formation and size from MK with heterozygous BSS, but not from homozygous BSS, under treatment with a ROCK1/2 inhibitor.

We report the first iPSC monoallelic BSS model derived from a patient with a new heterozygous mutation in the LRR4 domain of GPIbα, *GP1BA*^{N103D}. This mutation does not affect the expression of the GPIb-GPIX complex, DMS formation and GPIbα/FLNa interaction in contrast to previously described BSS models that rely on homozygous deletions in mice[4,5,30] or homozygous mutations in *GP1BB* and *GP1BA* in iPSC models,[7] leading to the absence or a profound decrease in GPIb complex expression at the cell surface and defects in DMS development. These findings suggest a different mechanism as in homozygous BSS, leading only to mild macrothrombocytopenia.

The abrogation of the GPIb-VWF interaction was demonstrated to affect proplatelet formation under shear, emphasizing the contribution of the extracellular domain of GPIb.[31] However, IL-4R/GPIbα-Tg mice, with an extracellular interleukin-4 receptor and an intracellular GPIbα cytoplasmic tail, partially restored platelet formation and platelet size compared to GPIbα-deficient mice,[13] suggesting that both intracellular and extracellular GPIbα domains are important for platelet generation.

This led us to hypothesize that point mutations in the extracellular domain of GPIbα and conserved intracellular domain in monoallelic BSS will affect inside-out signaling to αIIbβ3. A profound defect in PPF after adhesion on fibrinogen and increased stress fiber formation suggested an enhanced activation of the fibrinogen receptor αIIbβ3 and an overactivation of the RhoA pathway. Despite the

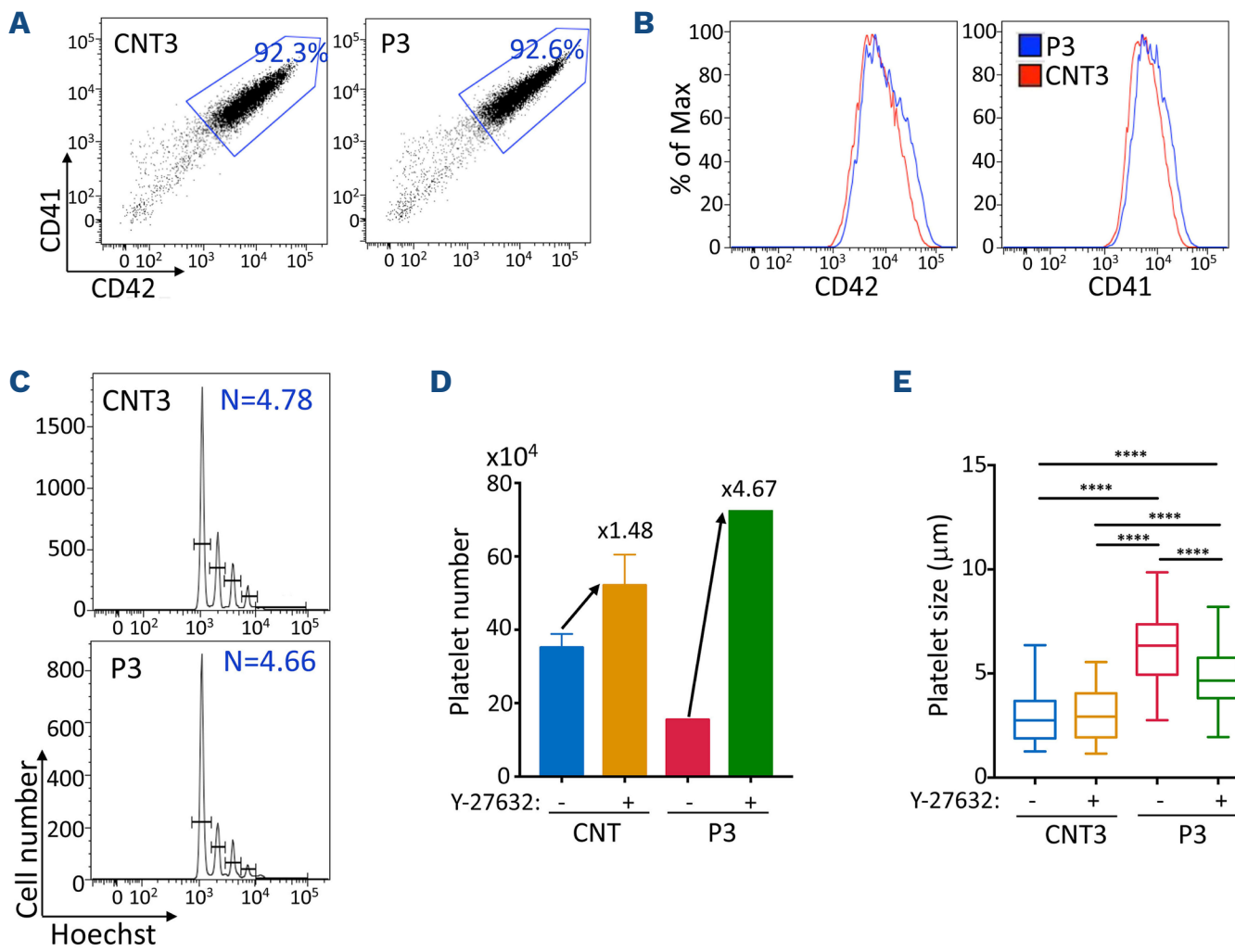

Figure 6. RhoA inhibition restores the platelet generation in heterozygous Bernard Soulier syndrome. Hematopoietic progenitors were isolated from peripheral blood of 3 healthy controls and 1 patient carrying heterozygous *GP1BA* p.N150S (P3) mutation respectively, and cultured in presence of thrombopoietin (TPO) and stem cell factor (SCF) for 10 days. (A-C) Flow cytometry analysis of control (CNT3) and patient 3 (P3) megakaryocytes (MK). (A) Percentage of mature CD41$^+$CD42$^+$ MK. (B) CD41 and CD42 expression level. (C) Ploidy level. CD41$^+$CD42$^+$ cells were incubated with Hoechst for 2 hours to label the nucleus. N represents a mean ploidy level. (D) MK were seeded into the silk scaffold with or without ROCK1/2 inhibitor Y27632. Silk scaffolds were perfused with culture media for 6 hours, and released platelets were collected into gas-permeable bags. Samples were mixed with counting beads to quantify the number of platelets, identified as CD41$^+$CD42a$^+$ events. The number of recovered platelets is shown. A 4.67-fold increase was detected for P3 after incubation with ROCK1/2 inhibitor. (E) Platelet diameters (mm) of *ex vivo*-released platelets with or without ROCK1/2 inhibitor Y27632 were measured by Arivis Vision 4D (Zeiss). Data are expressed as mean ± minimum to maximum, CNT N=57, CNT+Y27632 N=102, P3 N=57, P3+Y27632 N=57; ****P<0.0001, one-way analysis of variance (ANOVA) with Tukey's multiple comparison method was used.

absence of increased PAC-1 and fibrinogen binding at the steady state, their increased binding after activation by thrombin confirmed an increased αIIbβ3 pre-activation in the presence of the GPIb mutant. The enhanced RhoA activation after the adhesion of mutant MK on fibrinogen was probably due to increased signaling mediated by αIIbβ3. It is now well established that RhoA should be partially inactivated at the end of MK maturation to ensure normal thrombopoiesis,[32] and that GPIb controls a RhoA/CDC42 balance in this process,[26] which is clearly deregulated in the presence of the GPIbα^{N103D} mutant. As a result, the treatment of MK with a ROCK1/2 inhibitor not only decreased stress fiber formation but also restored PPF. Utilizing the recently described 3D silk-based bone marrow model,[18,19] which provides a favorable niche for thrombopoiesis, and includes a flow-through system that mimics the bloodstream to enable platelet release and collection, we demonstrated that treatment with a ROCK1/2 inhibitor not only restores the number of platelets generated but also their size.

In agreement with the basal RhoA activation, a slight effect of the ROCK1/2 inhibitor was also observed on healthy MK but was less pronounced than in mutant MK. Excessive acto-myosin contractility due to the overactivation of RhoA or its effectors leads to macrothrombocytopenia in MYH-9 syndrome[33] and in filaminopathy A.[16] Under normal conditions, FLNa maintains RhoA in an inactive state, and in its absence, RhoA becomes activated. However, in GPIbα^{N103D} MK, FLNa is normally localized, and no defect in the GPIbα-FLNa interaction is detected, suggesting that the mechanism of RhoA activation is different.

The cytoplasmic domain of GPIbα also interacts with the signal transduction molecule 14-3-3ζ,[11] which mediates the phosphorylation of many substrates in platelets. In MK, disruption of this interaction was shown to increase P-AKT levels, ploidization, and proliferation of MK.[12] However, the domain necessary for the interaction between GPIbα and 14-3-3ζ is conserved in the GPIbα^{N103D} mutant. Thus, to better understand the mechanism, proteomic arrays were performed and revealed increased phosphorylation in some proteins, including SRC at tyrosine Y419, which caught our attention. Indeed, SRC belongs to the Src family kinases that are associated with or in close proximity to αIIbβ3 and GPIb-GPIX receptors, transmitting signals to downstream effectors. Alongside Fyn and Lyn, SRC was shown to be implicated in the early stages of VWF-GPIb-GPIX mediated inside-out signaling to αIIbβ3 in platelets.[34,35] Through its direct interaction with the β3 subunit of αIIbβ3 integrin, SRC could also be involved in outside-in signaling after binding to fibrinogen.[36] Although VWF binding is required for GPIbα-mediated inside-out signaling in platelets, the GPIb-mediated signaling in MK is poorly understood. The affinity of VWF is decreased in the presence of GPIbα^{N103D} mutant, and this could lead to a defect in platelet release under shear[31] and thus participate to thrombocytopenia. However, no thrombocytopenia is observed in *vwf* KO mice,[6] and defects in platelet generation were observed in the absence of VWF, suggesting that the increased signaling is directly linked to the *GP1BA*^{N103D} mutation. The precise mechanism remains to be understood, but one of the explanations would be the induction of GPIb-GPIX receptor clustering leading to increased signaling to aIIbβ3 in the absence of VWF. Indeed, GPIb-GPIX clustering has been shown to increase adhesive function of aIIbβ3 after exposition to immobilized fibrinogen.[37]

Whether the increased phosphorylation of SRC on Y419 is directly mediated by mutant GPIbα^{N103D}, or indirectly as a consequence of GPIbα^{N103D}-induced pre-activation of αIIbβ3, or both, remains to be understood. Interestingly, SRC was shown to activate GEF-H1, the exchange factor involved in RhoA activation in MK,[38] by its release from microtubules. GEF-H1 activation could be mediated by SRC either directly[27] or indirectly through SRC-mediated phosphorylation of STAT3 on tyrosine Y705.[39,40,28,29] Therefore, the overactivation of RhoA could be a consequence of increased P-SRC Y419 downstream of GPIbα^{N103D}. According to this hypothesis, the SRC inhibitor dasatinib decreases stress fiber formation, however further studies are necessary to confirm GEF-H1 activation in presence of GPIba mutant.

Finally, the 3D silk-based model was employed to closely replicate the bone marrow structure and perfusion, allowing us to validate the restoration of platelet generation and size following ROCK1/2 inhibition for two other monoallelic BSS patients with *GP1BA* p.L160P and p.N150S mutations. Notably, the application of Y27632 had no additional impact on platelet generation from MK derived from two patients with biallelic BSS, as compared to control.

In conclusion, our findings indicate that monoallelic BSS is, at least in part, attributed to a defect in the late stages of megakaryopoiesis. This defect arises from dysregulated GPIbα-mediated VWF-independent signaling to aIIbβ3, leading to increased aIIbβ3 pre-activation, and increased SRC phosphorylation and RhoA activation after fibrinogen binding. In contrast, biallelic BSS involves different mechanisms, more closely aligning with the phenotype observed in *Gp1ba* and *Gp1bb* KO mice, which is characterized by a defect in DMS.

Disclosures

No conflicts of interest to disclose.

Contributions

LL, CADB, AK, NB, FB, CPMO, FC, IB, NP, TM and PR performed and analyzed experiments. CLB, VP, PB and RF provided patient samples. LL, CADB, AK, FB, IB, TM, PR, CLB, VP, PB, RF, IP, NP, SC, WV, AB and HR discussed results. HR supervised the work. LL, CADB, VW, IP, AB and HR wrote the article. LL and CADB equally contributed to this work. All the authors contributed to the final approval of the manuscript.

Acknowledgments

The authors thank the patients for participation in this study, M.C. Alessi who coordinates the "Centre de Référence des pathologies plaquettaires" (France); Sylvie Souquere from Electronic microscopy platform, UMS3655-AMMICA, Gustave Roussy Villejuif, France and Cyril Catelain from the Imaging and Cytometry Core Facility (PFIC) (Unit AMMICa, Gustave Roussy) for their expertise and advices in using instruments and methodological developments. Carolina P. Miguel, Matteo Migliavacca for technical assistance with confocal microscopy; Marco Lunghi for technical assistance with CAD design and 3D printing, 'Centro Grandi Strumenti' of the University of Pavia, Italy.

Funding

The work was supported by H2020-FETOPEN-1-2016-2017-SilkFusion (grant number 767309) and EIC Transition project SilkPlatelet (grant number 101058349) (to AB and HR) and by ANR-22-CE17-0043-01 MacroIT (to HR).

Data-sharing statement

Data generated in this study are available within this paper and upon request from the corresponding author. Any additional information required to reanalyze the data reported in this study is available from the corresponding author upon request.

References

1. Savoia A, Kunishima S, De Rocco D, et al. Spectrum of the mutations in Bernard-Soulier syndrome. Hum Mutat. 2014;35(9):1033-1045.
2. Ware J, Russell SR, Marchese P, et al. Point mutation in a leucine-rich repeat of platelet glycoprotein Ib alpha resulting in the Bernard-Soulier syndrome. J Clin Invest. 1993;92(3):1213-1220.
3. Noris P, Perrotta S, Bottega R, et al. Clinical and laboratory features of 103 patients from 42 Italian families with inherited thrombocytopenia derived from the monoallelic Ala156Val mutation of GPIbα (Bolzano mutation). Haematologica. 2012;97(1):82-88.
4. Poujol C, Ware J, Nieswandt B, Nurden AT, Nurden P. Absence of GPIbalpha is responsible for aberrant membrane development during megakaryocyte maturation: ultrastructural study using a transgenic model. Exp Hematol. 2002;30(4):352-360.
5. Strassel C, Eckly A, Léon C, et al. Intrinsic impaired proplatelet formation and microtubule coil assembly of megakaryocytes in a mouse model of Bernard-Soulier syndrome. Haematologica. 2009;94(6):800-810.
6. Denis C, Methia N, Frenette PS, et al. A mouse model of severe von Willebrand disease: defects in hemostasis and thrombosis. Proc Natl Acad Sci U S A. 1998;95(16):9524-9529.
7. Mekchay P, Ingrungruanglert P, Suphapeetiporn K, et al. Study of Bernard-Soulier syndrome megakaryocytes and platelets using patient-derived induced pluripotent stem cells. Thromb Haemost. 2019;119(9):1461-1470.
8. Aitken A. 14-3-3 and its possible role in co-ordinating multiple signalling pathways. Trends Cell Biol. 1996;6(9):341-347.
9. Muslin AJ, Tanner JW, Allen PM, Shaw AS. Interaction of 14-3-3 with signaling proteins is mediated by the recognition of phosphoserine. Cell. 1996;84(6):889-897.
10. Zha J, Harada H, Yang E, Jockel J, Korsmeyer SJ. Serine phosphorylation of death agonist BAD in response to survival factor results in binding to 14-3-3 not BCL-X(L). Cell. 1996;87(4):619-628.
11. Mangin PH, Receveur N, Wurtz V, David T, Gachet C, Lanza F. Identification of five novel 14-3-3 isoforms interacting with the GPIb-IX complex in platelets. J Thromb Haemost. 2009;7(9):1550-1555.
12. Kanaji T, Russell S, Cunningham J, Izuhara K, Fox JE, Ware J. Megakaryocyte proliferation and ploidy regulated by the cytoplasmic tail of glycoprotein Ibalpha. Blood. 2004;104(10):3161-3168.
13. Kanaji T, Russell S, Ware J. Amelioration of the macrothrombocytopenia associated with the murine Bernard-Soulier syndrome. Blood. 2002;100(6):2102-2107.
14. Jurak Begonja A, Hoffmeister KM, Hartwig JH, Falet H. FlnA-null megakaryocytes prematurely release large and fragile platelets that circulate poorly. Blood. 2011;118(8):2285-2295.
15. Begonja AJ, Pluthero FG, Suphamungmee W, et al. FlnA binding to PACSIN2 F-BAR domain regulates membrane tubulation in megakaryocytes and platelets. Blood. 2015;126(1):80-88.
16. Donada A, Balayn N, Sliwa D, et al. Disrupted filamin A/α(IIb)β(3) interaction induces macrothrombocytopenia by increasing RhoA activity. Blood. 2019;133(16):1778-1788.
17. Balduini A, Malara A, Pecci A, et al. Proplatelet formation in heterozygous Bernard-Soulier syndrome type Bolzano. J Thromb Haemost. 2009;7(3):478-484.
18. Di Buduo CA, Wray LS, Tozzi L, et al. Programmable 3D silk bone marrow niche for platelet generation ex vivo and modeling of megakaryopoiesis pathologies. Blood. 2015;125(14):2254-2264.
19. Di Buduo CA, Laurent PA, Zaninetti C, et al. Miniaturized 3D bone marrow tissue model to assess response to thrombopoietin-receptor agonists in patients. Elife. 2021;10:e58775.
20. Rockwood DN, Preda RC, Yücel T, Wang X, Lovett ML, Kaplan DL. Materials fabrication from Bombyx mori silk fibroin. Nat Protoc. 2011;6(10):1612-1631.
21. Di Buduo CA, Soprano PM, Tozzi L, et al. Modular flow chamber for engineering bone marrow architecture and function. Biomaterials. 2017;146:60-71.
22. Secardin L, Gomez Limia C, da Silva-Benedito S, et al. Induced pluripotent stem cells enable disease modeling and drug screening in calreticulin del52 and ins5 myeloproliferative neoplasms. Hemasphere. 2021;5(7):e593.
23. Saliba J, Hamidi S, Lenglet G, et al. Heterozygous and homozygous JAK2(V617F) states modeled by induced pluripotent stem cells from myeloproliferative neoplasm patients. PLoS One. 2013;8(9):e74257.
24. Antony-Debré I, Manchev VT, Balayn N, et al. Level of RUNX1 activity is critical for leukemic predisposition but not for thrombocytopenia. Blood. 2015;125(6):930-940.
25. Uff S, Clemetson JM, Harrison T, Clemetson KJ, Emsley J. Crystal structure of the platelet glycoprotein Ib(alpha) N-terminal domain reveals an unmasking mechanism for

receptor activation. J Biol Chem. 2002;277(38):35657-35663.
26. Dütting S, Gaits-Iacovoni F, Stegner D, et al. A Cdc42/RhoA regulatory circuit downstream of glycoprotein Ib guides transendothelial platelet biogenesis. Nat Commun. 2017;8:15838.
27. Azoitei ML, Noh J, Marston DJ, et al. Spatiotemporal dynamics of GEF-H1 activation controlled by microtubule- and Src-mediated pathways. J Cell Biol. 2019;218(9):3077-3097.
28. Pan YR, Chen CC, Chan YT, et al. STAT3-coordinated migration facilitates the dissemination of diffuse large B-cell lymphomas. Nat Commun. 2018;9(1):3696.
29. Joo E, Olson MF. Regulation and functions of the RhoA regulatory guanine nucleotide exchange factor GEF-H1. Small GTPases. 2021;12(5-6):358-371.
30. Ware J, Russell S, Ruggeri ZM. Generation and rescue of a murine model of platelet dysfunction: the Bernard-Soulier syndrome. Proc Natl Acad Sci U S A. 2000;97(6):2803-2808.
31. Dunois-Lardé C, Capron C, Fichelson S, Bauer T, Cramer-Bordé E, Baruch D. Exposure of human megakaryocytes to high shear rates accelerates platelet production. Blood. 2009;114(9):1875-1883.
32. Chang Y, Auradé F, Larbret F, et al. Proplatelet formation is regulated by the Rho/ROCK pathway. Blood. 2007;109(10):4229-4236.
33. Chen Y, Boukour S, Milloud R, et al. The abnormal proplatelet formation in MYH9-related macrothrombocytopenia results from an increased actomyosin contractility and is rescued by myosin IIA inhibition. J Thromb Haemost. 2013;11(12):2163-2175.
34. Senis YA, Mazharian A, Mori J. Src family kinases: at the forefront of platelet activation. Blood. 2014;124(13):2013-2024.
35. Wu Y, Asazuma N, Satoh K, et al. Interaction between von Willebrand factor and glycoprotein Ib activates Src kinase in human platelets: role of phosphoinositide 3-kinase. Blood. 2003;101(9):3469-3476.
36. Shattil SJ, Kim C, Ginsberg MH. The final steps of integrin activation: the end game. Nat Rev Mol Cell Biol. 2010;11(4):288-300.
37. Kasirer-Friede A, Ware J, Leng L, et al. Lateral clustering of platelet GP Ib-IX complexes leads to up-regulation of the adhesive function of integrin alpha IIbbeta 3. J Biol Chem. 2002;277(14):11949-11956.
38. Gao Y, Smith E, Ker E, et al. Role of RhoA-specific guanine exchange factors in regulation of endomitosis in megakaryocytes. Dev Cell. 2012;22(3):573-584.
39. Laird AD, Li G, Moss KG, et al. Src family kinase activity is required for signal tranducer and activator of transcription 3 and focal adhesion kinase phosphorylation and vascular endothelial growth factor signaling in vivo and for anchorage-dependent and -independent growth of human tumor cells. Mol Cancer Ther. 2003;2(5):461-469.
40. Garcia R, Bowman TL, Niu G, et al. Constitutive activation of Stat3 by the Src and JAK tyrosine kinases participates in growth regulation of human breast carcinoma cells. Oncogene. 2001;20(20):2499-2513.